A chip antenna in LTCC for UWB radios

Sun, Mei; Zhang, Yue Ping

2008

Sun, M., & Zhang, Y. P. (2008). A Chip Antenna in LTCC for UWB Radios. IEEE Transactions on Antennas and Propagation. 56(4), 1177-1180.

https://hdl.handle.net/10356/92683

https://doi.org/10.1109/TAP.2008.919216

Communications

A Chip Antenna in LTCC for UWB Radios

Sun Mei and Zhang Yue Ping

***Abstract*—The correspondence presents a chip antenna for ultrawideband (UWB) radios. The chip antenna is realized with a simple radiating element and small ground plane in low temperature cofired ceramic (LTCC) technology. The chip antenna has size $17 \times 8 \times 0.8\ \mathrm{mm}^3$ and achieves impedance bandwidth from 3.75 to 10.45 GHz and gain from −2 to 2.3 dBi over this frequency band. The measured radiation patterns are presented and small group-delay variations are found at the UWB frequencies from 3.1 to 10.6 GHz.**

***Index Terms*—Chip antennas, low temperature cofired ceramic (LTCC) technology, ultrawideband (UWB) antennas, wireless communications.**

I. Introduction

There is much interest today in developing ultrawideband (UWB) radios for short-range high-speed wireless communications. UWB radios exploit an ultrawide bandwidth of 7.5 GHz to exchange information. With such an ultrawide bandwidth, there exist challenges in making UWB radios up to its full potential. One of the major challenges is the antenna design, especially for use in handheld UWB radios. So far, there have been only a few attempts in the antenna design for handheld UWB radios [1]–[6]. Among them, the chip antenna design in low temperature cofired ceramic (LTCC) technology shows a promising future because a chip antenna provides the possibility of being automatically assembled and of being integrated with other circuits into a functional UWB radio [2]–[6]. In this correspondence, we present a chip antenna for UWB radios. The chip antenna is realized with a simple radiating element and small ground plane in LTCC. It is developed as an important step towards a highly-integrated solution of UWB radios [7]–[10]. The geometry and design guideline are described in Section II. The performances according to antenna usual criteria such as impedance bandwidth and radiation patterns are discussed in Section III. In addition, their performances based on measured transfer functions and impulse responses are also examined in Section III. Finally, the conclusions are summarized in Section IV.

II. Design of Chip Antenna in LTCC

Fig. 1 shows the geometry and the coordinate system of our chip antenna. As shown, the radiating element is a slotted patch with a bevel. It is fed with a half coplanar waveguide formed by the signal line and the ground plane. The radiating element, the ground plane, and the signal line are all printed on the same surface of a ceramic substrate with thickness h, dielectric constant of ε_r, and loss tangent δ. There is no ground on the back of the LTCC substrate.

Manuscript received November 6, 2006; revised October 3, 2007.

The authors are with the Integrated Systems Research Lab, School of Electrical and Electronic Engineering, Nanyang Technological University, Singapore 639798, Singapore (e-mail: sunmei@ntu.edu.sg).

Color versions of one or more of the figures in this paper are available online at http://ieeexplore.ieee.org.

Digital Object Identifier 10.1109/TAP.2008.919216

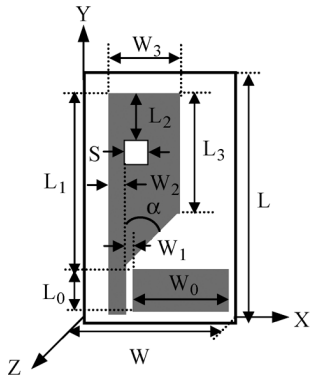

Fig. 1. Geometry and coordinate system of the chip antenna.

In designing the radiating element, the longest length of the patch L_1 is first estimated by

$$L_1 = \frac{c}{4 f_l \sqrt{\varepsilon_{\mathrm{eff}}}} \tag{1}$$

where c is the speed of light, f_l is the lowest operating frequency, and $\varepsilon_{\mathrm{eff}} = (\varepsilon_r + 1)/2$ is the effective dielectric constant [11]. The width and the shortest length of the patch W_3 and L_3 are then designed to optimize its impedance bandwidth. For a given width W_3 and W_2, the difference between the longest and shortest lengths of the patch determines the bevel angle α above the ground plane. A proper bevel angle can improve both impedance bandwidth and matching [12]. The patch has a square slot of side length S. The slot is primarily for the relief of stress from the different properties of metallic patch and ceramic substrate to avoid warpage or micro fracture of the antenna. For this mechanical purpose, the slot is added as the last design step and located at the place of the radiating patch with low surface current density. The size of the slot is so optimized as not to decrease the antenna electrical performance. The ground plane width W_0 should be maximized and the ground plane length L_0 should be co-designed with the signal line. The signal line and the ground plane form a half coplanar waveguide. In designing the half coplanar waveguide, we can assume that a mirrored half coplanar waveguide is added to create a full coplanar waveguide. Thus, the design formulas of the full coplanar waveguide can be applied to calculate the length L_0, the width W_2, and the gap W_1 of the half coplanar waveguide. Following this design guideline, we designed the chip antenna for UWB radios in LTCC from Ferro [13]. The Ferro ceramic type has a dielectric constant of 5.9 and a loss tangent smaller than 0.002 below 10 GHz. Two metallization options are gold and silver, of which silver metallization was chosen for our chip antennas. The simulation is conducted using HFSS. The designed geometric parameters of the chip antenna are $\mathrm{W} = 8\ \mathrm{mm}$, $\mathrm{W_0} = 6.7\ \mathrm{mm}$, $\mathrm{W_1} = 0.3\ \mathrm{mm}$, $\mathrm{W_2} = 1\ \mathrm{mm}$, $\mathrm{W_3} = 7\ \mathrm{mm}$, $\mathrm{h} = 0.8\ \mathrm{mm}$, $\mathrm{L} = 17\ \mathrm{mm}$, $\mathrm{L_0} = 3\ \mathrm{mm}$, $\mathrm{L_1} = 13\ \mathrm{mm}$, $\mathrm{L_2} = 5\ \mathrm{mm}$, $\mathrm{L_3} = 9\ \mathrm{mm}$, and $\mathrm{S} = 2\ \mathrm{mm}$.

III. Results and Discussion

The photograph of the fabricated chip antenna on a quarter U.S. dollar is shown in Fig. 2. The chip antenna was fed with the panel-mount SMA connector. The connector jack was soldered to the signal

Fig. 2. Photograph of the chip antenna in Ferro LTCC.

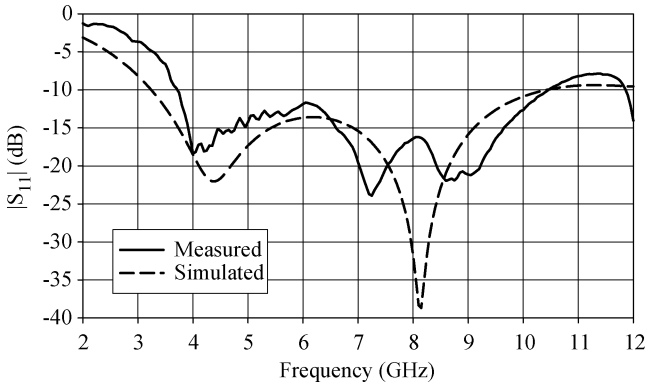

Fig. 3. Simulated and measured $|S_{11}|$ results.

line and the connector flange was soldered to the ground plane of the chip antenna. It should be noted that the connector ground extends the real antenna ground plane. The tests were conducted in an anechoic chamber with the S-parameter measured with an Agilent N5230A network analyzer and the radiation patterns with an HP 8510C network analyzer.

A. Bandwidth and Patterns

Fig. 3 shows the simulated and measured $|S_{11}|$ results. Using $|S_{11}| \leq -10$ dB as the threshold, the simulated impedance bandwidth is 7.2 GHz from 3.25 to 10.45 GHz while the measured impedance bandwidth is 6.7 GHz from 3.75 to 10.45 GHz. The discrepancy between the simulated and measured $|S_{11}|$ results was mainly caused by the soldering. It was found during the measurement that the $|S_{11}|$ result was very sensitive to soldering. The soldering was not included in the simulation.

Fig. 4 shows the simulated and measured radiation patterns in both E (YZ) and H(XZ) planes at 3.5 GHz, 6.85 GHz and 10 GHz, respectively. Note that the cross-polar radiation increases with frequency. At this point the simulated radiation patterns agree reasonably with the measured radiation patterns although the discrepancies exist between them. It is believed that the discrepancies were caused by the SMA connectors and the testing cables, which were not included in our simulations.

B. Transfer Function and Gain

To evaluate the transmission performance of the chip antenna (AUT), the measurement was conducted. During the measurement the transmitting antenna was fixed while the AUT or the standard antenna was mounted as the receiving antenna. The transmitting and receiving antenna pair was placed in an on-axis orientation with a separation distance of 1.6 m. In our measurement the WJ-48430 dual-polarized quad-ridged horn antenna was chosen to be both the transmitting and standard receiving antennas. This antenna has proved to be well matched to the measurement system from 3 to 18 GHz. The transmission scattering parameters $S_{21,\mathrm{AUT}}(f)$ and $S_{21,\mathrm{STD}}(f)$ were then measured by the N5230A network analyzer. It should be mentioned that the system was calibrated to the antenna terminals in advance.

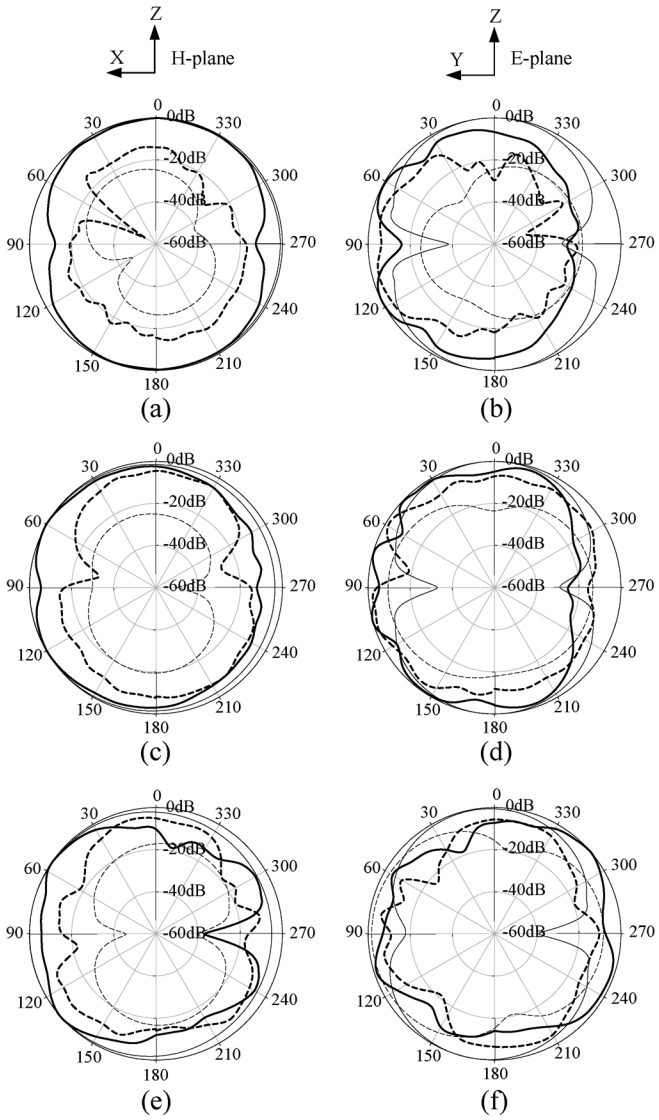

Fig. 4. Simulated and measured radiation patterns with solid lines for co-polarization components, short dash lines for cross-polarization components, normal lines for simulated results, and thicker lines for measured results: (a) H plane at 3.5 GHz, (b) E plane at 3.5 GHz, (c) H plane at 6.85 GHz, (d) E plane at 6.85 GHz, (e) H plane at 10 GHz, and (f) E plane at 10 GHz.

Fig. 5 shows the measured $S_{21,\mathrm{AUT}}(f)$ magnitude and group delay. The magnitude of the transmission scattering parameter is relatively flat and the group delay is relatively constant over the whole UWB frequency range. The normalized antenna transfer function of the AUT is further defined as follows to calibrate the range related effects [1]

$$H_{N,\mathrm{AUT}}(f) = \frac{S_{21,\mathrm{AUT}}(f)}{S_{21,\mathrm{STD}}(f)} H_{N,\mathrm{STD}}(f) \tag{2}$$

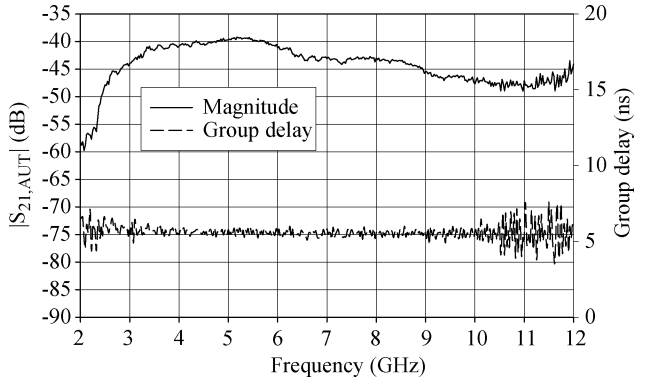

Fig. 5. Measured $S_{21,\mathrm{AUT}}(f)$ magnitude and group delay.

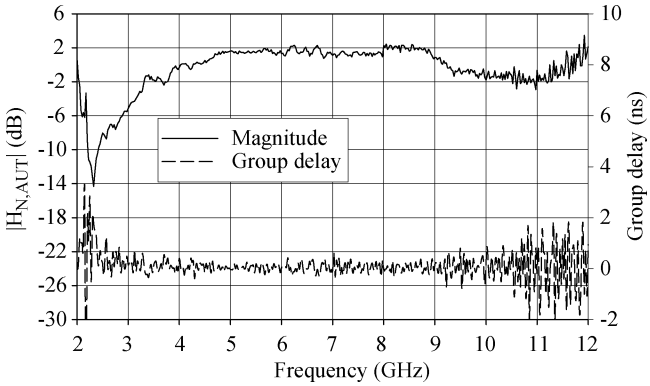

Fig. 6. Normalized antenna transfer function.

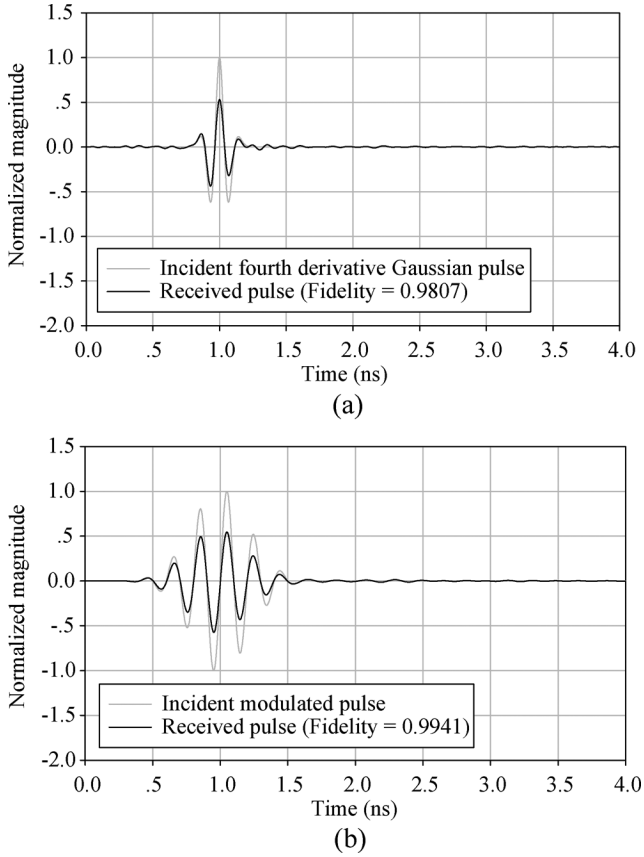

Fig. 7. Waveforms of the incident pulses and received pulses.

where $H_{N,\mathrm{SSTD}}(f)$ is the normalized antenna transfer function of the standard antenna. It can be readily achieved by referring to the gain data sheet and estimating group delay of the standard horn antenna as illustrated in [1]. Fig. 6 shows the $H_{N,\mathrm{AUT}}(f)$ magnitude and group delay. As expected, the magnitude of the normalized transfer function is relatively flat and the group delay is nearly constant over the frequency band of interest. It should be emphasized that the magnitude in decibels of the normalized transfer function is exactly the antenna absolute gain [1]. As seen from Fig. 6 that the gain varies from -2 to 2.3 dBi for the chip antenna over the whole frequency range of 3.75–10.45 GHz. As a consequence, the chip antenna has proved to be very suitable for UWB radios.

C. Time-Domain Characteristics

As the time-domain performance of an antenna is important for UWB radios, impulse response of the chip antenna is investigated. It is known that a UWB antenna should not introduce significant dispersion to the UWB pulse. The dispersion causes difficulties in distinguishing multipath signals and degrades the performance of correlation-based UWB receivers. Two kinds of incident pulse are selected in the investigation. One is the fourth derivative of a Gaussian pulse expressed as [1, Eq. (7)] with the parameters of $A = 0.1$ and $T_{au} = 175$ ps. The other is the modulated pulse expressed with carrier frequency $f_c = 5$ GHz and $\alpha = 300$ ps

$$s_i(t) = \sin(2\pi f_c t) e^{-\left(\frac{t}{\alpha}\right)^2}. \tag{3}$$

The waveforms of these two kinds of incident pulse are illustrated in Fig. 7. As seen in Fig. 8 their power spectrum density (PSD) comply with the required FCC indoor emission mask.

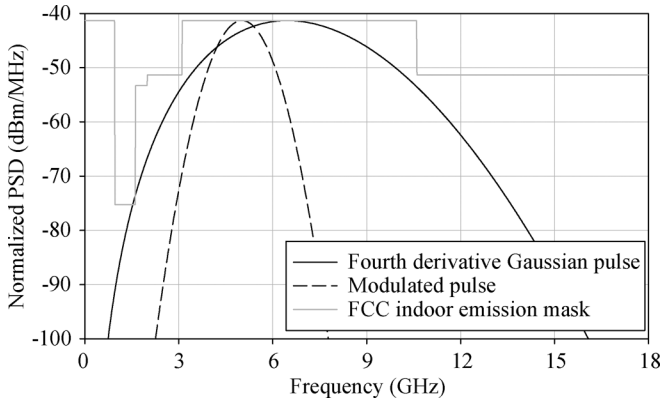

Fig. 8. The normalized PSD of the incident pulses.

The output waveform at the receiving antenna terminal can be expressed by an inverse Fourier transform as follows [1]:

$$s_r(t) = F^{-1}\left[s_i(f) H_{N,\mathrm{AUT}}(f) \Pi(f)\right] \tag{4}$$

where $\Pi(f)$ represents an ideal bandpass filter from 2 to 12 GHz. Fig. 7 also illustrates the received pulses by the chip antenna. The fidelity factor that evaluates the pulse distortion by the antenna is given in [1, Eq. (9)]. It reaches the maximum unity as the two pulses are exactly the same in shape. As shown in Fig. 7 with values of the fidelity factor better than 0.98 the well-behaved received pulses are demonstrated and the late time ringing is almost negligible. This validates that the chip antenna does not distort the transmitted pulse significantly. It also proves its applicability in pulse-based UWB radios.

TABLE I
PERFORMANCE SUMMARY OF THE CHIP ANTENNA AND COMPARISON WITH REPORTED STATE-OF-ART DESIGNS

UWB Chip Antennas	Technology	Radiator	Radiator & FN* Size	Ground Size	Bandwidth	Peak Gain	Gain Flatness
This work	Single-layer LTCC	Metal patch	17×8×0.8	16×6	3.75-10.45	2.3	7.9
[2]	Single-layer LTCC	Metal patch	10×5×1	30×30	3.1-10.6	0.8	10.12
[3]	Multi-layer LTCC	Metal patch	14×10×1.5	80×50	2.39-7.75	3.8	2
[4]	Multi-layer LTCC	unknown	8×6×1	25×20	3.1-10.6	unknown	unknown
[5]	Multi-layer LTCC	unknown	8×8×0.8	unknown	3.1-10.6	1.7	unknown

Dimension in millimeters (mm), bandwith in gigahertz (GHz), gain in dBi, and its flatness in decibels (dB). * FN (Feeding Network)

Table I shows a summary of measured performances of our chip antenna. The comparison with other reported state-of-the-art chip antennas is also presented. Here it should be mentioned that other designs using different voltage standing wave ratio (VSWR) values to define their impedance bandwidths. $\mathrm{VSWR} < 2.3$, 2.5, 2.4, and 2.5 are used respectively, in [2]–[5]. It is shown that our chip antenna has good performance and can be produced in large quantity using a simpler single-layer LTCC technology. As the radiating element and the ground is printed on the surface of the ceramic substrate, the performance of our chip antennas can be easily adjusted even after the antenna has been manufactured and assembled.

IV. CONCLUSION

This correspondence described the design guideline and examined the performance of a novel chip antenna for UWB radios. The chip antenna was realized with a simple radiating element and small ground plane in LTCC from Ferro. The chip antenna of size $17 \times 8 \times 0.8\ \mathrm{mm}^3$ achieved impedance bandwidth from 3.75 to 10.45 GHz and gain from -2 to 2.3 dBi over this frequency band. The measured radiation patterns are presented and small group-delay variations are found at the UWB frequencies from 3.1 to 10.6 GHz. Further development of the chip antenna into a chip package is being carried out in our laboratory for a highly-integrated solution of UWB radios.

ACKNOWLEDGMENT

The authors would like to thank Mr. K. M. Chua of Singapore Institute of Manufacturing Technology for his help in fabricating the antennas and their colleague Mr. S. H. Wi for his help in measuring the antenna.

REFERENCES

[1] T. G. Ma and S. K. Jeng, "Planar miniature tapered-slot-fed annular slot antennas for ultrawide-band radios," *IEEE Trans. Antennas Propag.*, vol. 53, no. 3, pp. 1194–1202, Mar. 2005.
[2] D. H. Kwon, Y. J. Kim, M. Hasegawa, and T. Shimamori, "A small ceramic chip antenna for ultra-wideband systems," in *Proc. IEEE UWBST*, May 2004, pp. 307–311.
[3] C. Y. Wu, C. L. Tang, and A. C. Chen, "UWB chip antenna design using LTCC multilayer technology for mobile applications," in *Proc. IEEE APMC*, Dec. 2005, vol. 3, pp. 1493–1495.
[4] [Online]. Available: http://www.ntktech.com/Antenna/Antenna_PDF/
[5] [Online]. Available: http://www.trda-inc.com/
[6] Y. J. Zheng, Y. P. Zhang, and Y. Tong, "A novel wireless interconnect technology using impulse radio for inter-chip communications," *IEEE Trans. Microw. Theory Tech.*, vol. 54, no. 4, pp. 1912–1920, Apr. 2006.
[7] C. Ying and Y. P. Zhang, "A planar antenna in LTCC for single-package ultrawide-band radio," *IEEE Trans. Antennas Propag.*, vol. 53, no. 9, pp. 3089–3093, Sep. 2005.
[8] Y. Chen and Y. P. Zhang, "Integration of ultra-wideband slot antenna on LTCC substrate," *Electron. Lett.*, vol. 40, pp. 645–646, Mar. 2004.
[9] Y. P. Zhang, "Finite-difference time-domain analysis of integrated ceramic ball grid array package antenna for highly integrated wireless transceivers," *IEEE Trans. Antennas Propag.*, vol. 52, no. 2, pp. 435–442, Feb. 2004.
[10] Y. P. Zhang, "Integration of microstrip antenna on cavity-down ceramic ball grid array package," *Electron. Lett.*, vol. 38, no. 22, pp. 1307–1308, Sep. 2002.
[11] S. B. Cohn, "Slot line on a dielectric substrate," *IEEE Trans. Microw. Theory Tech.*, vol. 17, no. 10, pp. 768–778, Oct. 1969.
[12] M. J. Ammann, "Control of the impedance bandwidth of wideband planar monopole antennas using a beveling technique," *Microw. Opt. Technol. Lett.*, vol. 30, no. 4, pp. 229–232, August 2001.
[13] [Online]. Available: http://www.ferro.com

High Isolation Proximity Coupled Multilayer Patch Antenna for Dual-Frequency Operation

Luis Inclán-Sánchez, José-Luis Vázquez-Roy, and Eva Rajo-Iglesias

***Abstract*—A new method to enhance the isolation between two ports in a dual-frequency proximity coupled patch antenna is presented. The dual-polarized patch antenna has a multilayer substrate configuration to achieve a compact design. In addition, two periodic structures have been included under the two feeding lines to have stopband behavior in the other frequency port. These electromagnetic bandgap (EBG) filters have been realized by introducing mushroom type resonators underneath the antenna feeding lines. Measurements show how the isolation between the feeding ports can be improved by selecting a suitable size for the resonators. The proposed antenna design achieves an isolation higher than 55 dB in the first frequency band (2.1 GHz) and better than 40 dB in the second one (2.45 GHz). Radiation patterns are not affected by the proposed structures showing low cross-polarization levels in both planes at the two frequency bands.**

***Index Terms*—Dual frequency, dual polarization, electromagnetic bandgap (EBG) filter, high isolation, patch antenna, proximity coupling.**

I. INTRODUCTION

Dual-frequency dual-polarization patch antennas have been subject of study in the last two decades [1]–[3]. The dual-polarization dual-frequency concept is becoming useful for multiple reasons. In communication applications the increasing demand for high-speed data links has produced the emergence of multiband wireless access systems. As a result, low cost integration of multiband devices, based on a single radiator becomes highly desirable for compact communication systems and multifunction operation [4]. This is the case of the recent concept

Manuscript received February 8, 2007; revised June 29, 2007. This work was supported by the Spanish Ministry of Science and Technology under project TIC2003-03808.

The authors are with the Signal Theory and Communication Department, University Carlos III of Madrid, 28911 Leganés (Madrid), Spain (e-mail: linclan@tsc.uc3m.es).

Digital Object Identifier 10.1109/TAP.2008.919218